Lawrence Berkeley National Laboratory
Recent Work

Title
THE STRUCTURE AND IMPURITY PINNING OF SUBGRAIN BOUNDARIES IN AS-GROWN MgO

Permalink
https://escholarship.org/uc/item/47g8w3cx

Author
Narayan, J.

Publication Date
1973

eScholarship.org Powered by the California Digital Library
University of California

Submitted to Physica Status Solidi

LBL-828
Preprint

THE STRUCTURE AND IMPURITY PINNING OF SUBGRAIN BOUNDARIES IN AS-GROWN MgO

J. Narayan

January 1973

Prepared for the U. S. Atomic Energy Commission
under Contract W-7405-ENG-48

For Reference

Not to be taken from this room

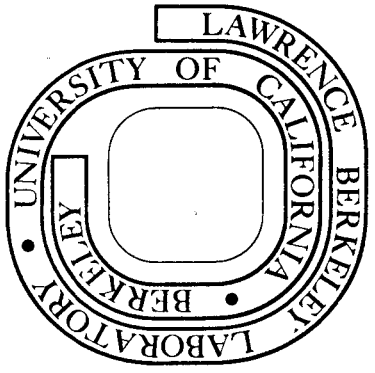

LBL-828

DISCLAIMER

This document was prepared as an account of work sponsored by the United States Government. While this document is believed to contain correct information, neither the United States Government nor any agency thereof, nor the Regents of the University of California, nor any of their employees, makes any warranty, express or implied, or assumes any legal responsibility for the accuracy, completeness, or usefulness of any information, apparatus, product, or process disclosed, or represents that its use would not infringe privately owned rights. Reference herein to any specific commercial product, process, or service by its trade name, trademark, manufacturer, or otherwise, does not necessarily constitute or imply its endorsement, recommendation, or favoring by the United States Government or any agency thereof, or the Regents of the University of California. The views and opinions of authors expressed herein do not necessarily state or reflect those of the United States Government or any agency thereof or the Regents of the University of California.

0 0 0 0 3 8 0 3 7 1 1

THE STRUCTURE AND IMPURITY PINNING OF SUBGRAIN BOUNDARIES IN AS-GROWN MgO

J. Narayan†

Inorganic Materials Research Division, Lawrence Berkeley Laboratory and Department of Materials Science and Engineering, College of Engineering; University of California, Berkeley, California

ABSTRACT

The structure of subgrain boundaries in as-grown MgO has been characterized using transmission electron microscopy. The subboundaries were found to consist of one set $\frac{1}{2}$ [101], two sets $\frac{1}{2}$ [101] and $\frac{1}{2}$ [011] or three sets of dislocations: A, b-vector $\frac{1}{2}$ [101]; B, b-vector $\frac{1}{2}$ [011]; and C, b-vector $\frac{1}{2}$ [10$\bar{1}$]. At the nodes the following dislocation reactions occur: $\frac{1}{2}$ [011] + $\frac{1}{2}$ [10$\bar{1}$] = $\frac{1}{2}$ [110] and $\frac{1}{2}$ [10$\bar{1}$] + $\frac{1}{2}$ [101] = [100]. The role of impurities in pinning the subboundaries is discussed.

†Present address: Solid State Division, Oak Ridge National Laboratory, Oak Ridge, Tennessee 37830.

INTRODUCTION

When a large mass of MgO is cooled slowly from the melt to produce large grains, most of the grains contain subgrain boundaries. During cooling, thermal stresses may result in some slip dislocations joining the boundaries. Therefore, the two-dimensional dislocation network which comprises the subgrain boundary is often complex. The geometry of two-dimensional dislocation networks in crystals of the NaCl type was studied from the theoretical point of view by Frank.[1] Amelinckx[2] observed some of the dislocation nets in NaCl using decoration techniques. Washburn et al.[3] observed dislocation reactions in MgO by transmission electron microscopy. The purpose of this paper is to analyze the structure of subgrain boundaries in MgO in detail and establish the various dislocation reactions that occur during formation of the two-dimensional dislocation array. The effect of impurity precipitates on the local subboundary structure is also investigated.

EXPERIMENTAL

Polycrystalline MgO in the form of large grains was obtained from Muscle Shoals Electrochemical Corporation, Tuscumbia, Alabama. Semi-quantitative spectrographic analysis revealed the following impurities (in ppm): Al-200, Si-200, Fe-30; all other elements were undetected.

Thin sheets containing at least two grains were cleaved on {100} faces. Specimens were first chemically polished in 85% orthophosphoric acid at 150-160°C to a thickness of about 0.4 mm. Final thinning of areas near grain boundaries was done using a jet polishing technique.[3]

0 0 0 0 3 8 0 0 7 1 2

RESULTS AND DISCUSSION

In MgO (NaCl structure) there is only one <110> slip direction in each {110} slip plane. Since there are six {110} slip planes, dislocations of the following b-vectors are possible: $\frac{1}{2}$ [110], $\frac{1}{2}$ [1$\bar{1}$0]; $\frac{1}{2}$ [011], $\frac{1}{2}$ [0$\bar{1}$1]; $\frac{1}{2}$ [101], $\frac{1}{2}$ [$\bar{1}$01].

Figure 1 shows a simple tilt boundary. It consists of two sets of parallel dislocations, ones with dark contrast having higher image width than others. Both sets are in contrast for diffraction vector g = [200]. The boundary is invisible for g = [020]. Therefore dislocations have either b = $\frac{1}{2}$ [101] or b = $\frac{1}{2}$ [$\bar{1}$01]. The dislocations A, B, C, and D are very near to screw orientation and others are nearly edge. The character of the dislocations can be assessed from the image width of the dislocations[4] (explained below). Since the boundary is pure tilt, the screw components of dislocations A, B, C, and D should just cancel the screw components of all the other dislocations. The tilt boundary is in the (101) plane and the axis of rotation is [10$\bar{1}$] in this plane. The sub-boundary angle can be determined from the measurements of the shift in Kikuchi lines across the boundary and using the relation:

$$\Delta\theta = 2\,\theta\,\left(\frac{|\Delta g|}{|g|}\right) \qquad (1)$$

where θ is the Bragg angle of diffracting planes, $|\Delta g/g|$ is the fractional change in the diffraction vector g. $|\Delta g/g| \sim 1.4$ (Fig. 1) and substituting λ/d (λ = 0.037 Å for 100 keV electrons) for 2θ in the above equation, we get $\Delta\theta \sim 0.2°$. The sub-boundary angle can also be calculated

from Frank's formula:

$$\bar{d} = (\bar{r} \times \bar{u})\ 2\ \mathrm{Sin}\ \frac{\theta}{2} \cong (\bar{r} \times \bar{u})\theta \quad , \qquad (2)$$

$\bar{r}$ is an arbitrary vector lying in the plane of the boundary with the axis of rotation $\bar{u}$, $\bar{d}$ is the sum of Burgers vectors of the dislocations intersected by $\bar{r}$ and θ is the sub-boundary angle. The second expression is valid for small angles only. From this equation the sub-boundary angle is calculated to be about 0.1°. The disagreement between the two values of sub-boundary angle might be partly due to charging of the specimen inside the microscope which can also cause shifting of Kikuchi lines.

Figure 2 shows a sub-boundary consisting of A and B sets of dislocations. Figure 2c is the continuation of the boundary in Fig. 2a and b inside the crystal. The few dislocations which run across the boundary will be designated as set C. For diffraction vector g = [200] sets A and C are in good contrast (see Fig. 2a). The faint contrast associated with the set B will be explained later. However, for g = [020] (Fig. 2b) only set B is in contrast. For g = [220] (Fig. 2c) all the sets A, B, and C are in good contrast. Applying the g·b criterion[5] for visibility of dislocations and in view of the following facts, we can assign Burgers vectors to all three sets unambiguously: Sets A and B must have repulsive interaction, otherwise the boundary will be unstable. That this is true can be seen at 1 in Fig. 2a. Sets B and C have an attractive interaction (see at 2 in Fig. 2a). Therefore a consistent set of b-vectors which can be assigned to sets A, B, and C is $\frac{1}{2}$ [101], $\frac{1}{2}$ [011], and $\frac{1}{2}$ [10$\bar{1}$] respectively. The dislocation reactions consistent with the

0 0 0 0 3 8 0 0 7 1 3

above are:

$$\frac{1}{2}\,[101]_{A} + \frac{1}{2}\,[011]_{B} \rightarrow \frac{1}{2}\,[112] \text{ at } 1 \quad ,$$

$$\frac{1}{2}\,[011]_{B} + \frac{1}{2}\,[10\bar{1}]_{C} \rightarrow \frac{1}{2}\,[110] \text{ at } 2 \quad ,$$

$$\frac{1}{2}\,[101]_{C} + \frac{1}{2}\,[10\bar{1}]_{A} \rightarrow [100] \text{ at } 3 \quad .$$

A further confirmation of the assignment of Burgers vectors is the contrast at the nodes at 3 in Fig. 2a. The dark contrast on one side and the faint contrast on the other side of the node show that the images of dislocations lie on opposite sides. From the kinematical theorem of image contrast, the image of a dislocation lies closer to the Bragg condition. Since the b-vectors of A and C sets are at 90°, the Bragg condition will be close in opposite directions and the observed contrast will result.

When dislocations are parallel, one can show from Frank's formula that they form a pure tilt boundary. In this case we can choose a direction such that no dislocation lines will be intersected. From Frank's formula, then $\bar{r} \times \bar{u} = 0$, i.e., the dislocation lines are parallel to the axis of rotation of the boundary and therefore the boundary is a pure tilt boundary (see Fig. 2). The plane of the boundary in Fig. 2 is (112), which is in agreement with the electron microscope observation. This is in fact the extension of a boundary predicted theoretically by Frank[1] (see Fig. 11 of this reference). The axis of rotation is $[11\bar{1}]$.

The sub-boundaries in Figs. 3 and 4 also consist of three sets of dislocations A, B, and C. However, the number of C-type dislocations is more than that in the boundary in Fig. 2. These are no longer pure tilt boundaries, but have both tilt and twist components. The plane of the boundary is slightly rotated from the (112) plane toward the $(11\bar{1})$ plane. However, the axis of rotation is still $[11\bar{1}]$. The dislocation reactions of the types 1, 2, and 3 occur at various places in Figs. 3 and 4.

The strain fields around the impurities at the boundaries interact with dislocations and also act as dislocation sources. Note the impurities at 4, 5, and 6 in Figs. 2, 3, and 4 and their interactions with the sub-boundaries.

The residual contrast of B dislocations for $\bar{g}$ = [200] can be explained on the basis of the kinematical theory of electron diffraction contrast.[5] Since the Burgers vector of the B set is $\frac{1}{2}$ [011], $\bar{g}\cdot\bar{b}$ for $\bar{g}$ = [200] is equal to zero, but the observable contrast might result from the $\bar{g}\cdot\bar{b}\times\bar{u}$ component ($\bar{u}$ is the tangent vector of the dislocation). Also a weakly excited diffraction vector for which $\bar{g}\cdot\bar{b}$ is not zero can result in such observable contrast. Howie and Whelan[4] computed the contrast from mixed dislocations and showed that when g (diffraction vector) lies in the plane of the foil, the image is characterized by a parameter $p = \frac{2}{3(1-\nu)} \frac{\bar{g}\cdot\bar{b}_e}{\bar{g}\cdot\bar{b}}$ (ν = Poisson's ratio, b_e is the edge component of the total Burgers vector b). They found that the image of a pure edge dislocation is wider than that of a pure screw by a factor of about two. The sets A and B have high edge components, i.e., $\theta \cong 60°$ (θ is the angle between the dislocation line and its b-vector) whereas the set C has a high screw component, i.e., $\theta \cong 19°$.

The dislocation (B + C) at the type 2 nodes has $\theta = 65°$ and the dislocation (C + A) at the type 3 nodes has $\theta = 70°$.

The equilibrium angles at nodes are determined by the line tensions of the constituting dislocations which in turn depend upon their nature. From the isotropic elastic theory,[6] the energy per unit length of a mixed dislocation is:

$$E = Ab^2(1 - \nu \cos^2\theta) \quad , \tag{3}$$

where $A = \mu \ln(r_1/r_o)/4\pi(1-\nu)$ in which μ is the shear modulus and r_1 and r_o are the cut-off radii of the elastic stress field. Neglecting the dislocation interaction energies, a simple balance of line tensions at the type 2 nodes gives the angle between B and C dislocations as 126° against the observed value of 135°. The discrepancy between the observed and theoretical values is presumably due to the use of isotropic elastic theory[7] and the fact that core energy and dislocation-dislocation interaction terms have not been accounted for in the calculations.

Perhaps these observations provide the best evidence for a type 3 dislocation reaction (see at 3 in Figs. 2, 3, and 4). Here the gain in energy comes only from the sharing of cores with high atomic misfit. This is, in general, insignificant for metals but in ionic crystals due to high atomic disorder near the core region, the gain in energy is quite appreciable. Using decoration techniques Amelinckx[8] reported this type of reaction in KCl crystals.

CONCLUSION

The sub-grain boundaries have been characterized in MgO on the basis of the kinematical theory of electron diffraction. Three distinct types of boundaries have been observed:

(1) Pure tilt boundary consisting of $\frac{1}{2}[101]$ dislocations on (101) plane with the axis of rotation $[10\bar{1}]$;

(2) Pure tilt boundary consisting of mainly two sets of dislocations A, $b = \frac{1}{2}[101]$ and B, $b = \frac{1}{2}[011]$ on (112) plane with the axis of rotation $(11\bar{1})$;

(3) Mixed boundary with three sets of dislocations A, $b = \frac{1}{2}[101]$; B, $b = \frac{1}{2}[011]$; C, $b = \frac{1}{2}[10\bar{1}]$ on the plane close to (112) with the axis of rotation $(11\bar{1})$. The hexagonal and square networks observed by Amelinckx[2] in rock salt using decoration techniques can be formed by B and C sets, and C and A sets respectively.

The occurrence of the following dislocation reactions in MgO has been directly confirmed:

$$\frac{1}{2}[011] + \frac{1}{2}[\bar{1}0\bar{1}] = \frac{1}{2}[110] \quad ,$$

and

$$\frac{1}{2}[10\bar{1}] + \frac{1}{2}[101] = [100] \quad .$$

The strain field around the impurities promotes the interaction and this interaction may render the boundaries relatively immobile.

0 0 0 0 0 3 8 0 0 7 1 4

ACKNOWLEDGMENTS

The author isgrateful to Prof. J. Washburn and Dr. S. M. Ohr for stimulating discussions. Thanks are also due to Drs. T. Noggle, V. K. Paré and H. D. Guberman for useful comments on the manuscript.

This work was done under the auspices of the U. S. Atomic Energy Commission through the Inorganic Materials Research Division of the Lawrence Berkeley Laboratory, Berkeley, California.

REFERENCES

1. F. C. Frank, Proc. Phys. Soc. (Report of Bristol Conference, 1954) p. 159 (1955).
2. S. Amelinckx, Phil. Mag. 1, 269 (1956).
3. J. Washburn, G. W. Groves, A. Kelly and G. K. Williamson, Phil. Mag 5, 991 (1960).
4. A. Howie and M. J. Whelan, Proc. Roy. Soc. A267, 206 (1962).
5. P. B. Hirsch et al., Electron Microscopy of Thin Crystals, Butterworths (1965).
6. A. H. Cottrell, Dislocations and Plastic Flow in Crystals, p. 51, Oxford University Press, 1953.
7. J. P. Hirth and J. Lothe, Theory of Dislocations, p. 681, McGraw-Hill Book Co., 1968.
8. S. Amelinckx, Acta Met. 6, 34 (1958).

0 0 0 0 3 8 0 0 / 1 3

FIGURE CAPTIONS

Fig. 1. Pure tilt boundary of $\frac{1}{2}$ [101] dislocations. Note the smaller image width of A, B, C, and D dislocations which are very near to screw orientation and shifting of Kikuchi lines across the sub-boundary.

Fig. 2. Pure tilt boundary with $\frac{1}{2}$ [101] and $\frac{1}{2}$ [011] dislocations.

(a) g = [200], A set in contrast. Note the residual contrast with the B set, and inside and outside contrast at 3. Repulsive interaction is occurring at 1.

(b) g = [020], B set in contrast. The residual contrast of [100] segments at 3 is due to their high edge component.

(c) Continuation of the boundary in 2a and b; g = [220], all dislocations in contrast. Impurity-dialocation interactions may be seen.

Fig. 3. Mixed boundary with Burgers vectors $\frac{1}{2}$ [101], $\frac{1}{2}$ [011] and $\frac{1}{2}$ [10$\bar{1}$], d signated as A, B and C sets of dislocation

(a) a = [200], A and C sets are in contrast. Note the repulsive interactions at 1, attractive interactions at 2, and residual contrast of the B set. The reactions at 3 occur primarily because of gain in core energy.

(b) g= [020], only B set in contrast, the residual contrast is associated with [100] segments at 3. Note the dislocation impurity pinning.

Fig. 4. (a) $g = [\bar{2}00]$, A and C sets are in contrast. The dislocation reactions of 1, 2, and 3 types are shown. Notice also the residual contrast with the B set.

(b) $g = [020]$, only B set is in contrast, the residual contrast is associated with [100] segments at 3. Note the impurity-dislocation interactions at 4, 5, and 6.

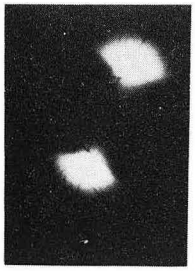

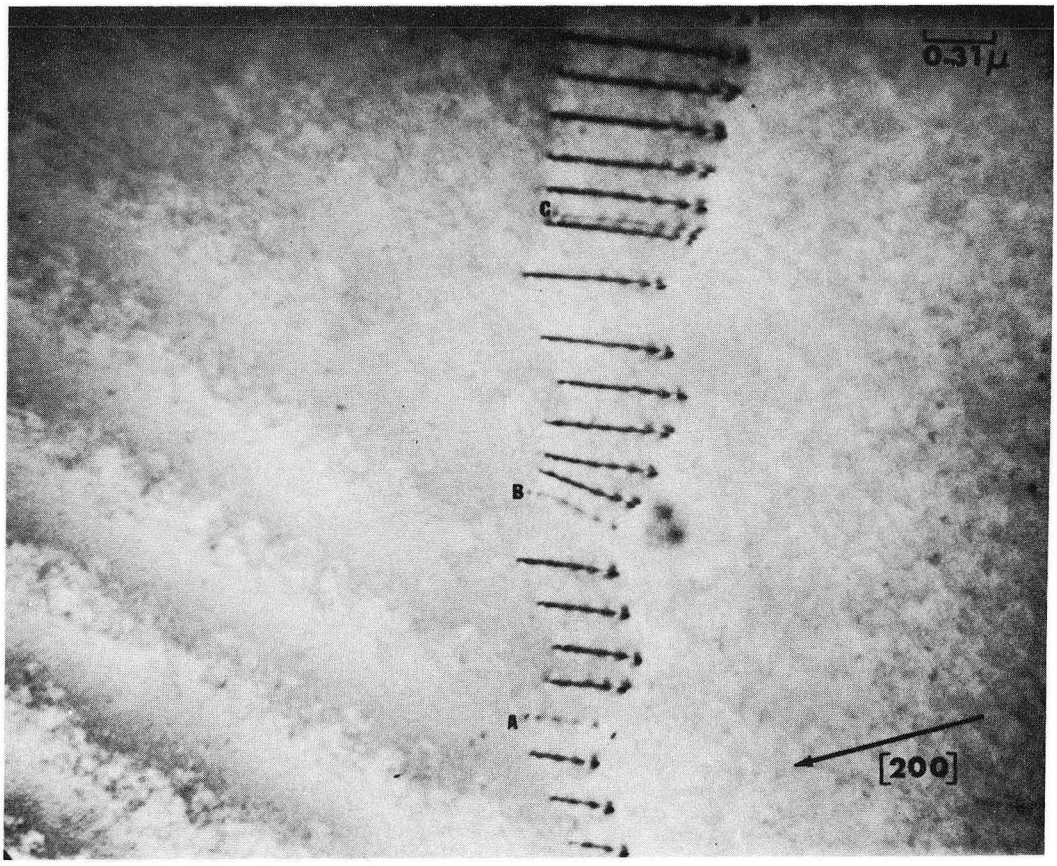

XBB 724-2198

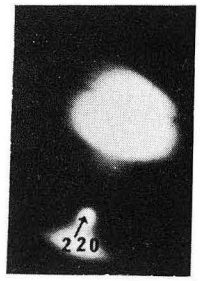

Fig. 1.

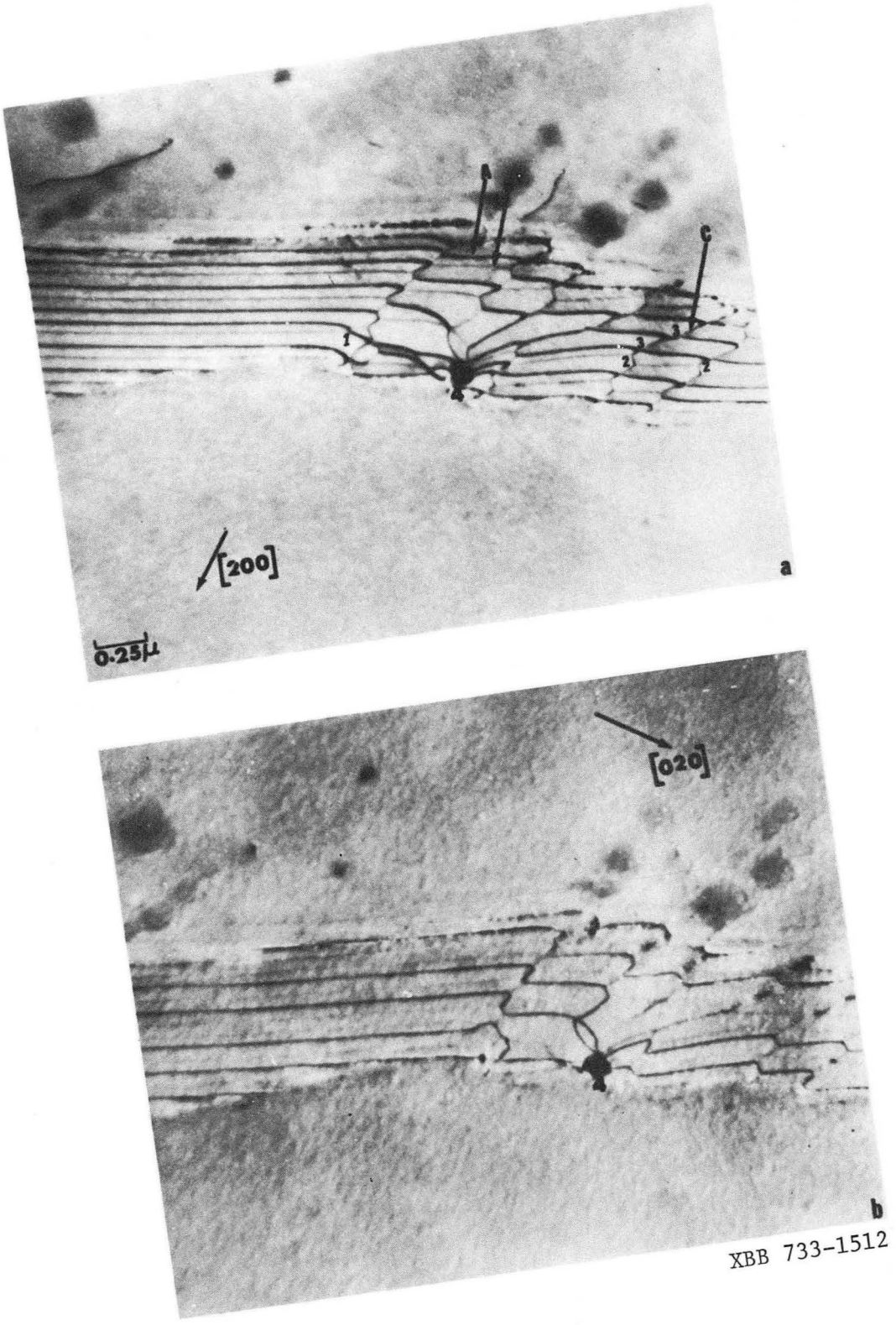

XBB 733-1512

Fig. 2(a) and (b).

0 0 0 0 3 8 0 0 7 1 6

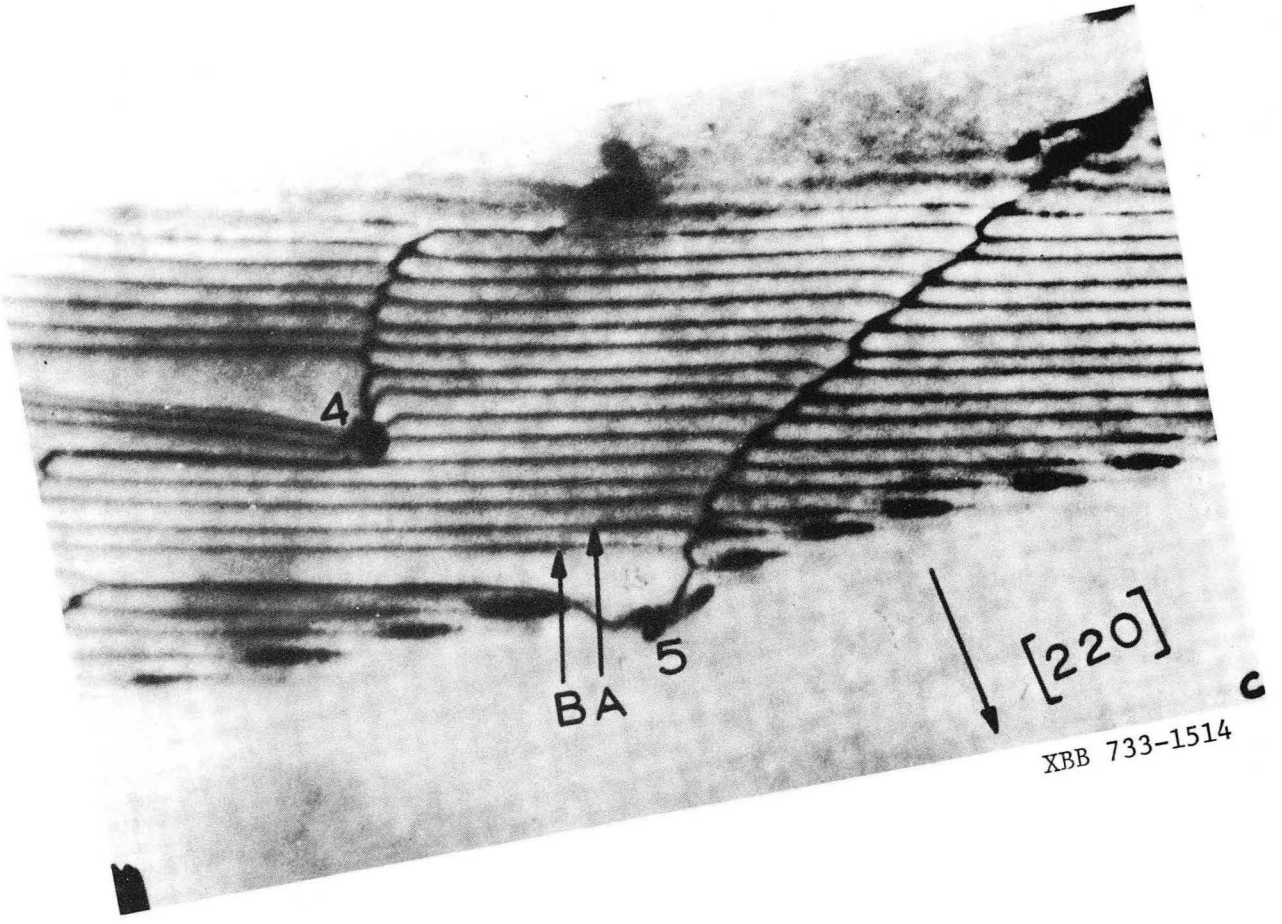

Fig. 2(c).

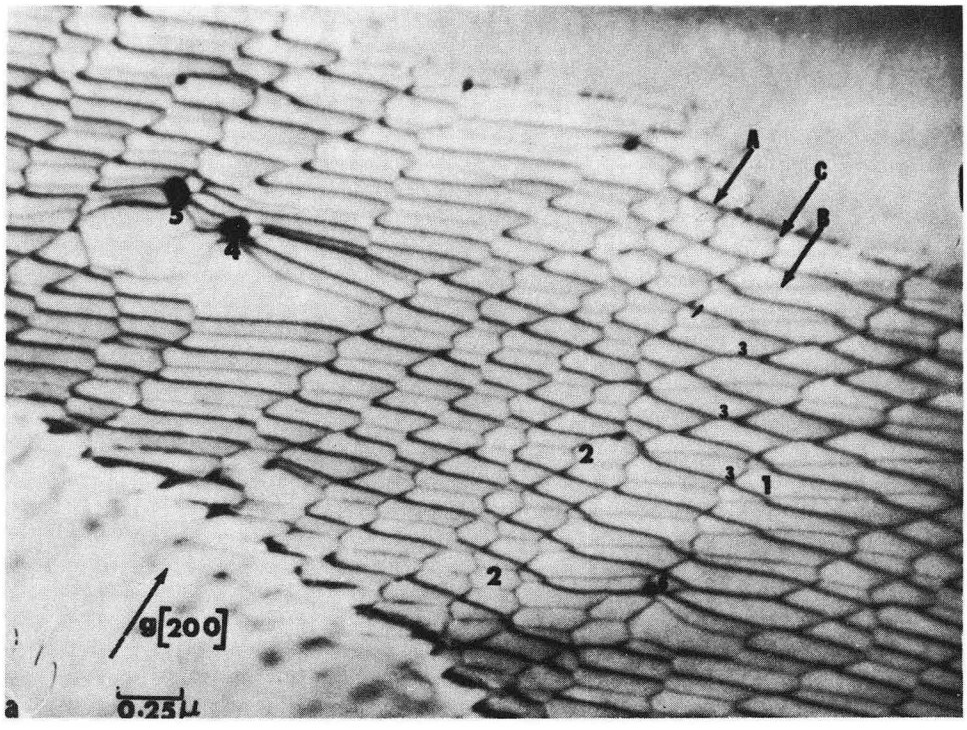

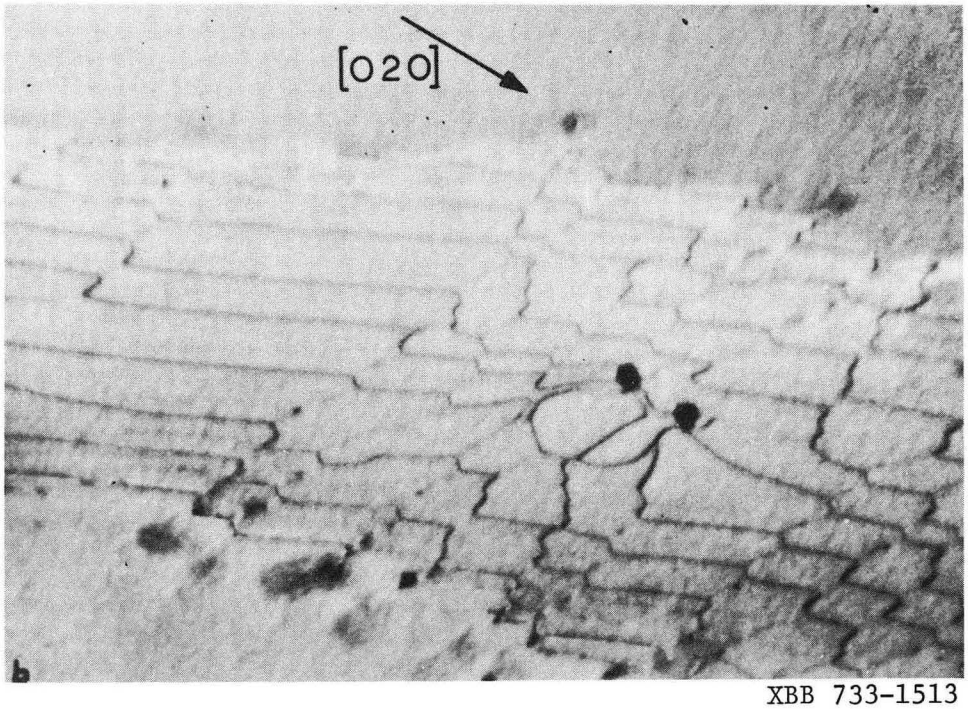

XBB 733-1513

Fig. 3.

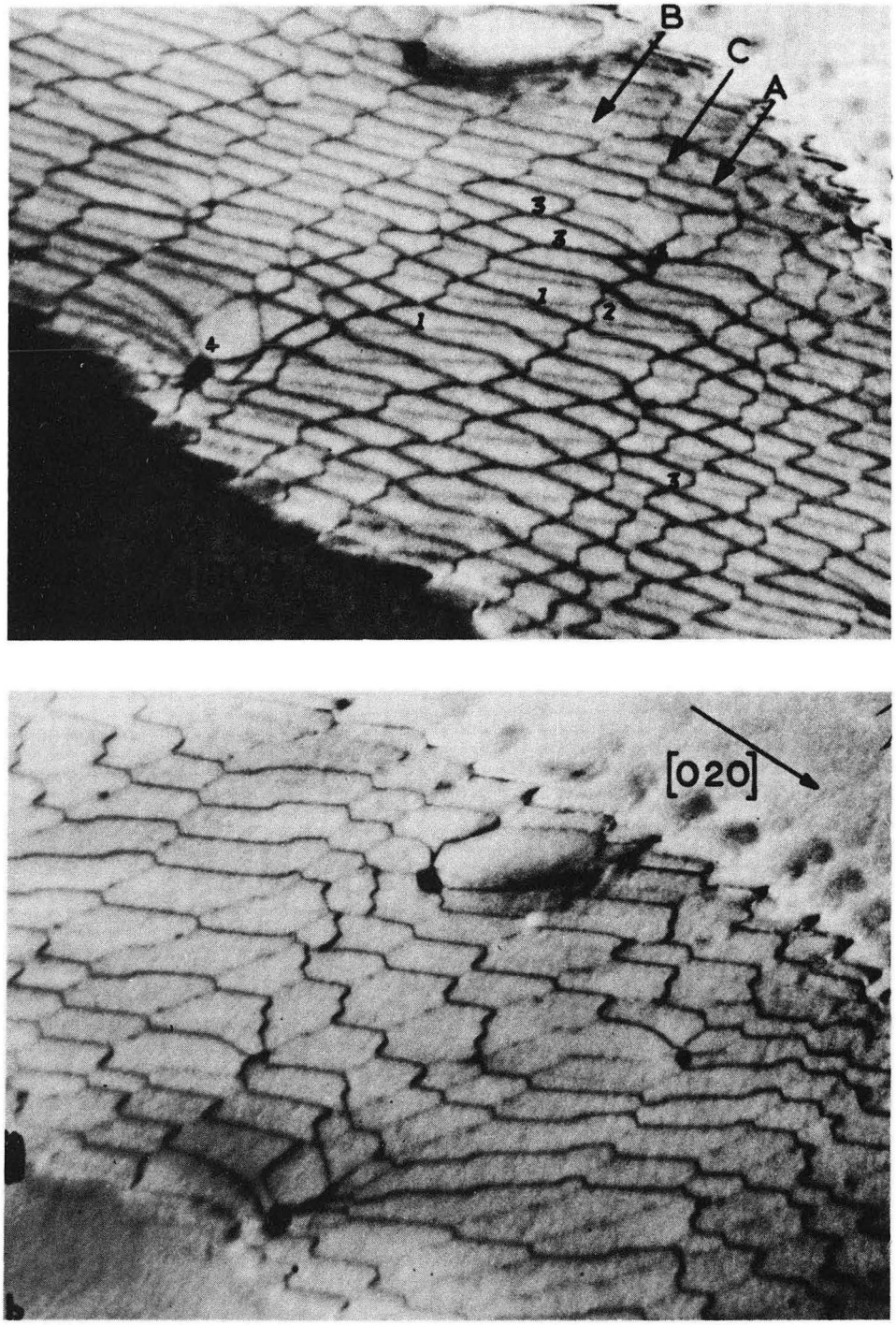

XBB 733-1511

Fig. 4.

LEGAL NOTICE

This report was prepared as an account of work sponsored by the United States Government. Neither the United States nor the United States Atomic Energy Commission, nor any of their employees, nor any of their contractors, subcontractors, or their employees, makes any warranty, express or implied, or assumes any legal liability or responsibility for the accuracy, completeness or usefulness of any information, apparatus, product or process disclosed, or represents that its use would not infringe privately owned rights.

TECHNICAL INFORMATION DIVISION
LAWRENCE BERKELEY LABORATORY
UNIVERSITY OF CALIFORNIA
BERKELEY, CALIFORNIA 94720